Received: 15 January 2020 | Revised: 19 March 2020 | Accepted: 3 April 2020

DOI: 10.1002/ldr.3620

WILEY

RESEARCH ARTICLE

Mapping erosion risk for saline rangelands of the Mancos Shale using the rangeland hydrology erosion model

Kenneth C. McGwire[1] | Mark A. Weltz[2] | Sayjro Nouwakpo[2] | Ken Spaeth[3] | Michael Founds[4] | Erik Cadaret[5]

[1]Division of Earth and Ecosystems Sciences, Desert Research Institute, Reno, Nevada

[2]Great Basin Rangelands Research Unit, USDA Agricultural Research Service, Reno, Nevada

[3]Central National Technology Support Center, USDA National Resources Conservation Service, Fort Worth, Texas

[4]cbec eco engineering, West Sacramento, California

[5]Water Systems Consulting, San Luis Obispo, California

Correspondence
Kenneth C. McGwire, Division of Earth and Ecosystems Sciences, Desert Research Institute, Reno, Nevada.
Email: kenm@dri.edu

Funding information
Agricultural Research Service, Grant/Award Number: 59-2060-6-001; US Bureau of Land Management, Grant/Award Number: 60-5370-4-001

Abstract

This research used the rangeland hydrology and erosion model (RHEM) to map erosion risks affecting water quality of the Colorado River that originate on the Mancos Shale formation in Utah, Colorado, New Mexico, and Arizona. The Mancos Shale is a significant source of salinity to the river, and a portion of that salt load derives from erosion of rangeland soils. Here we demonstrate that the hillslope-scale RHEM model can effectively characterize erosion risk across this large, discontinuous region. Inputs to RHEM included digital elevation data, maps of soil properties, the LANDFIRE vegetation map, Landsat and MODIS satellite imagery, field data from the Rangeland National Resource Inventory program of the US Natural Resources Conservation Service, and rainfall data from Atlas 14 of the U.S. National Atmospheric and Oceanographic Administration. RHEM predicted sediment yield at a 30-m spatial resolution for storms with 30- and 60-min durations whose intensities corresponded to 10- and 25-year return frequencies. Results corresponded reasonably with prior field experiments that used the Walnut Gulch Rainfall Simulator (WGRS), with a Spearman's rank-order correlation of .76 for cumulative sediment yield after 20 min of rainfall. Issues of input map accuracy were identified for rainfall intensity and estimates for sodium adsorption ratio (SAR) of soils. Correction of erroneous SAR at WGRS sites in one location improved rank-order correlation to .93, indicating very good model performance where map inputs are accurate. The high-resolution map of erosion risk developed from RHEM can help to prioritize specific areas for more intensive study and action.

KEYWORDS

Colorado River, erosion, LANDSAT, sodic, sodium adsorption ratio, water quality

1 | INTRODUCTION

Nineteen percent of non-federal rangelands in the state of Utah in the United States are experiencing moderate to extreme departures from historic reference conditions simultaneously for soil stability, hydrologic function, and biotic integrity (NRCS, 2018). Some of these degraded lands are located on saline soils of the Mancos Shale formation, contributing disproportionate amounts of sediment, salinity, and selenium to the Colorado River (Spahr et al., 2000; USBOR, 2013). The Colorado River is a critical resource for the United States and Mexico, and its water quality is subject to treaty obligations between the countries. Land management agencies in the United States are considering mitigation activities to reduce erosion on these saline rangelands, and an initial question is how to prioritize different locations for action. Prior work has documented a significant linear relationship between salinity and sediment in the runoff from

experimental rainfall simulator plots on the saline Mancos Shale formation (Cadaret, McGwire, Nouwakpo, Weltz, & Saito, 2016; Cadaret, Nouwakpo, McGwire, Weltz, & Blank, 2016; Nouwakpo, Weltz, Arslan, Green, & Al-Hamdan, 2018), and that work demonstrates the potential for using erosion models to predict salinity loads from these rangelands under varying conditions of soil, topography, vegetation, and rainfall. The work presented here provides a map of erosion rates for soils of the Mancos Shale at a 30-m resolution. This map can serve as part of a prioritization effort to identify specific regions of elevated erosion risk for possible mitigation activities.

Outcrops of the Mancos Shale extend discontinuously through Wyoming, Utah, Colorado, New Mexico, and Arizona, with most of their area draining to the Colorado River. The various units of the Mancos Shale were laid down during the Mid-Late Cretaceous in near-shore environments of the Western Interior Seaway. As such, the bedrock and soils of the Mancos Shale are saline, and sometimes sodic depending on the depositional environment. Natural sources have long been recognized as a major source of salinity in the UCRB, with Iorns, Hembree, and Oakland (1965) attributing 60% to natural sources and 40% to agriculture. Using the SPARROW model, Kenney, Gerner, Buto, and Spangler (2009) found a very similar proportion and quantified the great importance of 'high-yield' saline sedimentary formations from the Mesozoic like the Mancos Shale. There have been changes in agriculture and land use in the UCRB over time, with irrigated agriculture on the Mancos Shale likely becoming a dominant contributor to river salinity (Tuttle, Fahy, Elliott, Grauch, & Stillings, 2014). Despite this, a contemporaneous study by the U.S. Bureau of Reclamation (2013) still attributes almost half (47%) of salinity within the Colorado River to natural sources.

A variety of surface and subsurface processes move salts from the rangelands of the Mancos Shale to the Colorado River. Prior studies estimate that as much as 55% of the salinity in the Colorado River is from groundwater and subsurface reemergence (Kenney et al., 2009; Shirnian-Orlando & Uchrin, 2000; Warner, Heimes, & Middelburg, 1985). In addition to groundwater salinity from the geological substrates, Miller, Buto, Lambert, and Rumsey (2017) revisited prior work by Kenney et al. (2009) with the SPARROW model and found salinity from rangelands in the entire UCRB to be on the order of 30 tons per square mile. It is likely that the saline load is larger for rangeland soils derived from saline geological parent material compared to other geologic formations in the UCRB. In fact, the outline of the Mancos Shale is quite visible as the areas of highest rangeland salt yields in Figure 5 of that report. Using new high-resolution soil datasets that they developed statistically, Nauman, Ely, Miller, and Duniway (2019) applied random forest regression to predict salinity sources in the upper Colorado River basin (UCRB) with a 30-m grid resolution. One of the most consistent predictors of salinity in that effort was an index of bare ground, particularly in mountainous terrain. Tillman, Anning, Heilman, Buto, and Miller (2018) assessed the degree to which different reaches in the UCRB might be candidates for mitigating salinity by reducing or capturing soil erosion. While no simple relationship provided a uniform result across the UCRB, many stream gauge locations that were predicted to be good candidates for mitigation coincided with drainages where the Mancos Shale is present. Since that effort focused on the stream network, hillslope erosion models would be required to identify the best field locations for actual mitigation activities.

A common approach for estimating erosion has been to use the universal soil loss equation (USLE; Wischmeier & Smith, 1978), or its various modifications (MUSLE, RUSLE, RUSLE2) that provide empirical estimates of long-term erosion rates. However, these empirical methods have important limitations and do not correctly reflect hillslope-scale soil erosion process on rangelands (Kinnell, 2005; Weltz, Kidwell, & Fox, 1998; Spaeth, Pierson, Weltz, & Blackburn, 2003). Furthermore, the soils data required to provide the K-factor or C-factor in USLE-derived equations are not available for large portions of the Mancos Shale or UCRB. In contrast, a process-based model provides a more sound basis for predictions in new environments, as well as the ability to test multiple scenarios for environmental conditions and management actions. This is because its mechanistic formulation is less tied to the explicit circumstances of a prior empirical relationship. However, compared to the simple algebraic formulations of empirical techniques, implementation of a dynamic, process-based erosion model for the entire Mancos Shale would consume more time and computational resources. This article presents a method for mapping erosion potential across the Mancos Shale at a high spatial resolution using the rangeland hydrology and erosion model (RHEM; Nearing et al., 2011). RHEM acts at the hillslope-scale to estimate localized erosion rates, so it requires less effort than models that compute flow and transport through the larger hydrologic network. This allows easy implementation across the discontinuous spatial extent of Mancos Shale outcrops because it does not consider the continuity of mass and energy balances or boundary conditions beyond the single cells of the grid of input data values. Here, RHEM is parameterized with existing geospatial datasets, satellite imagery, and field data from the National Resource Inventory (NRI) dataset collected by the United States Department of Agriculture (USDA) National Resources Conservation Service (NRCS). This approach produces maps of erosion risk that can help land managers to define thresholds of accelerated soil loss, to assess the risk of crossing such a threshold, and to define hot spots where soil conservation can be applied to avert land and water degradation.

2 | MATERIALS AND METHODS

The study area was the extent of Mancos Shale outcrops that were compiled from maps of surface geology for Utah, Colorado, New Mexico, and Arizona (Figure 1). The region under consideration was limited to areas with low levels of agricultural or urban development and slopes less than 35%. These constraints reflect practical limitations for potential mitigation activities; also, the RHEM model is not well validated for very steep slopes. Data for developed land uses and slope were taken from the LANDFIRE vegetation map (140EVC attribute class numbers <100, except 31; USGS, 2017) and the United States Geological Survey (USGS) 1/3 arc sec National Elevation Database (USGS, 2002). All map datasets for the study were raster grids that

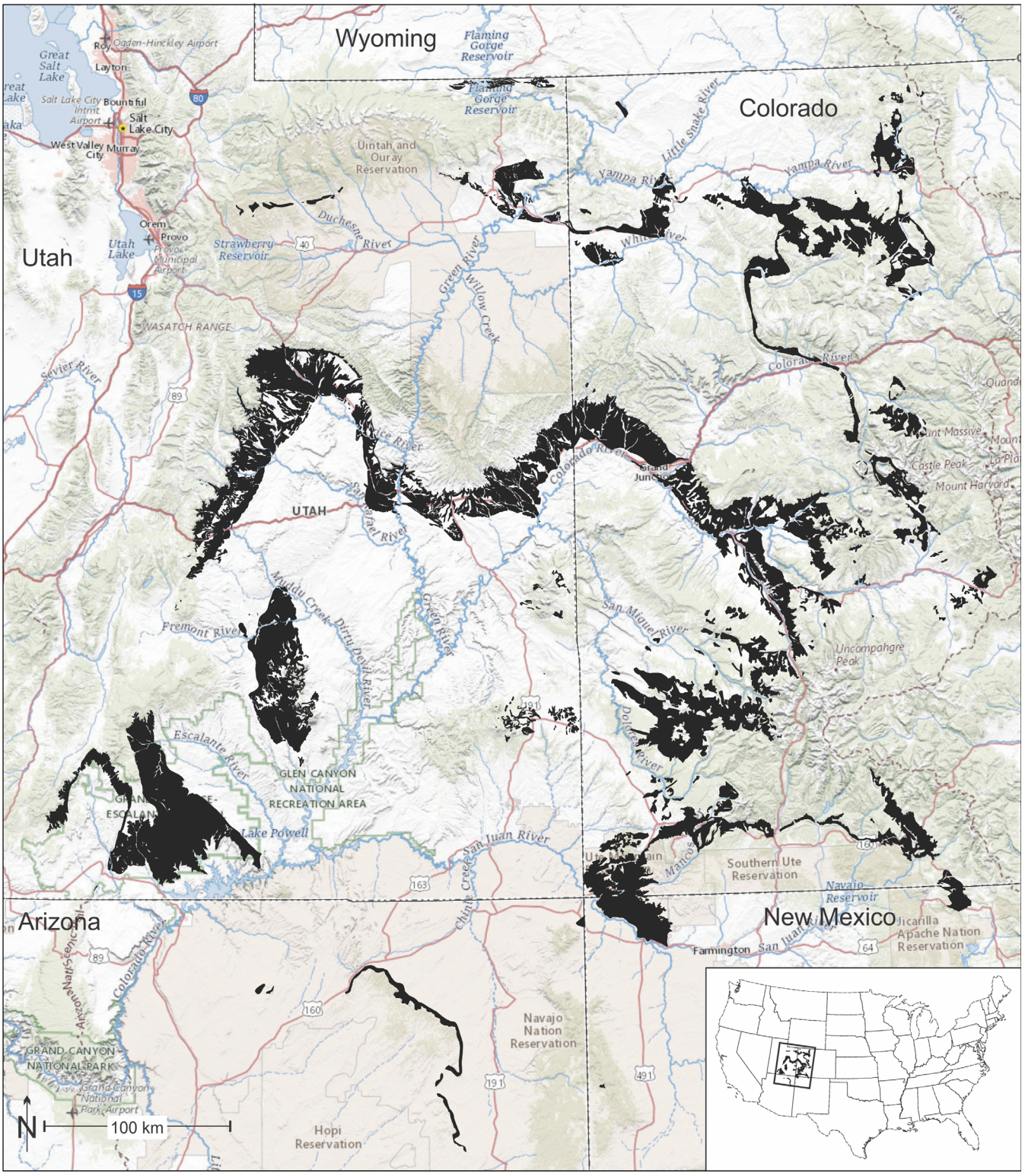

FIGURE 1 The Mancos Shale (black) in Utah, Colorado, Arizona, and New Mexico (terrain reference: USGS National Map) [Colour figure can be viewed at wileyonlinelibrary.com]

were projected to UTM Zone 12 with the NAD83 datum at a 30-m spatial resolution.

For vegetation, RHEM requires estimates of percent cover by (a) annuals and forbs, (b) bunch grasses, (c) sod grasses, (d) shrubs, (e) litter (on ground), (f) basal area (rooted plant area), and (g) biological crusts. Given the arid to semiarid climate of the study area, sod grasses were not considered. Also, data on the distribution of biological crusts throughout the region were not available and

assumed to be zero. This assumption is revisited in Section 4. Remaining foliar and ground cover values were estimated on a per-pixel basis using a combination of field transect data from the NRI, satellite imagery, and the LANDFIRE vegetation map. Maps of percent vegetation cover were created by developing a regression relationship between available field transect data and collocated values of the normalized difference vegetation index (NDVI; Rouse, Haas, Schell, Deering, & Harlan, 1974) from LANDSAT satellites. That relationship was then applied to Landsat NDVI data (30-m spatial resolution) for areas that were mapped as Mancos Shale, as described below.

Plant foliar and ground cover data was obtained from the USDA-NRCS NRI nonfederal rangeland on-site field study (NRCS, 1997). NRI data are collected as two 50 m transects, oriented 45° from north (NE–SW; NW–SE), with point-intercept samples every 0.9 m (Spaeth, Pierson, Herrick, Shaver, Pyke, et al., 2003). These crossed transects are randomly located in ecosystems around the United States. Hernandez, Nearing, Stone, Pierson, Wei, et al. (2013) found that NRI data were adequate to run RHEM and to effectively assess the influence of foliar cover, ground cover, plant life forms, soils, and topography on soil erosion rates in desert environments of the southwestern United States. The NRI data used here were from 134 crossed transects that were collected from 2004 to 2014 at locations that were within 1 km of the mapped distribution of the Mancos Shale. Total vegetation cover was estimated by developing a regression between total cover at NRI locations and the corresponding median of Landsat NDVI collected during the growing season (April–September) of that year (Figure 2a). Pearson's correlation (*r*) between these two variables was .834. The analysis compensated for changes in Landsat bandwidths from the earlier Thematic Mapper sensor to the current Operational Land Imager (OLI) sensor using the method of Huntington et al. (2016). A Type II regression technique called reduced major axis (RMA) regression was used, since ordinary least squares regression would produce a deflated slope estimate due to measurement uncertainty in the independent variable (Curran & Hay, 1986; McGwire, Friedl, & Estes, 1993). The median of NDVI data derived from LANDSAT during the 2018 growing season was converted to 30-m scale estimates of percent cover across the Mancos Shale (Figure 3a) for RHEM using the regression in Figure 2a.

The proportion of shrub cover for each pixel (Figure 3b) was taken from the 140EVC attribute in version 1.4 of the LANDFIRE map which used an algorithm to estimate tree or shrub cover that was based on the example of Toney, Shaw, and Nelson (2009). Tree cover classes in the 140EVC attribute were treated as shrubs in the RHEM model. The shrub and tree cover attributes in LANDFIRE are reported at 10% intervals, so the midpoint of each interval was used (e.g., 10–20% = 15%). To test of the accuracy of these cover classes, combined shrub and tree cover in NRI transects was compared to the corresponding LANDFIRE pixels. The difference in the overall average between the two sources was 4.4%, indicating low overall bias. On average, the midpoint of each LANDFIRE cover class was 0.69 standard normal deviates from the mean of NRI cover values. In the very rare case that the LANDFIRE shrub/tree cover class exceeded the LANDSAT regression estimate for total cover, the regression value was used for total cover and shrub cover since it was developed specifically from data for the local environs. For estimating proportions of annuals and forbs versus bunch grasses with NRI data, a simple area-wide mean performed as well as any predictive relationship to satellite data or vegetation type. The mean proportion of the two categories was very similar in the NRI dataset, so Landsat-estimated cover that was in excess of the LANDFIRE shrub cover was split evenly between these two classes. The NRI dataset did demonstrate a useful relationship between litter and total plant cover (r = .709; Figure 2b), and this was applied using a RMA regression with the Landsat estimate of plant cover. For basal area, a weak relationship to total plant cover (r = .13) was all that could be derived from the NRI dataset (Figure 2c). Attempts using NRI to predict basal areas based on life form (i.e., shrub, bunch grass, etc.) were no better than the single relationship in Figure 2c. Estimated values of foliar and ground cover were truncated if they exceeded the range of 0–100%.

Slope for the RHEM model (Figure 3c) was taken from the 1/3 arc sec National Elevation Dataset which has spatial resolution of approximately 10 m. Slope calculations are sensitive to interpolation

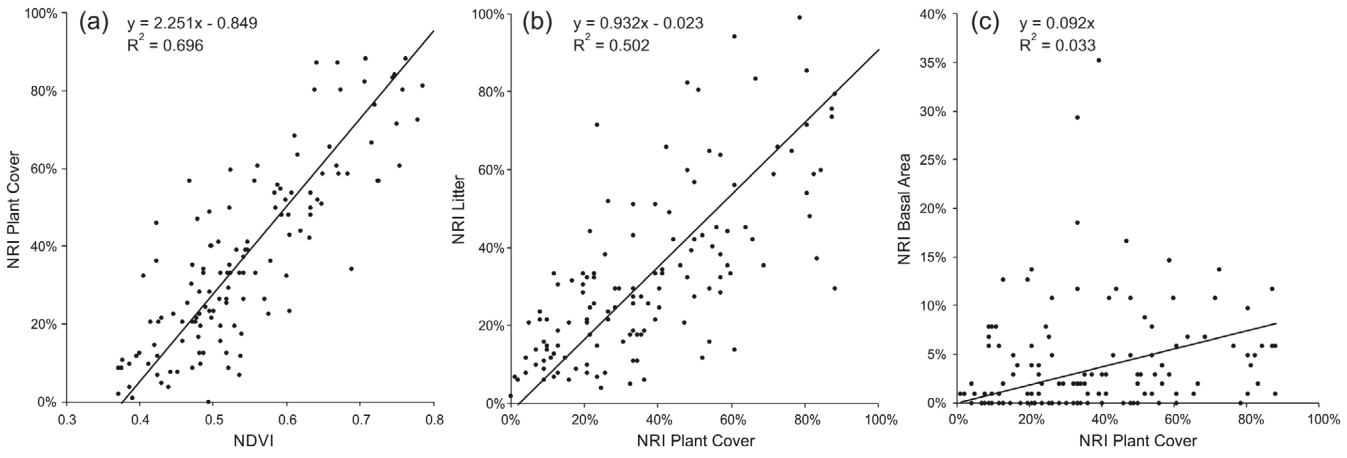

FIGURE 2 Regressions for estimating vegetation variables

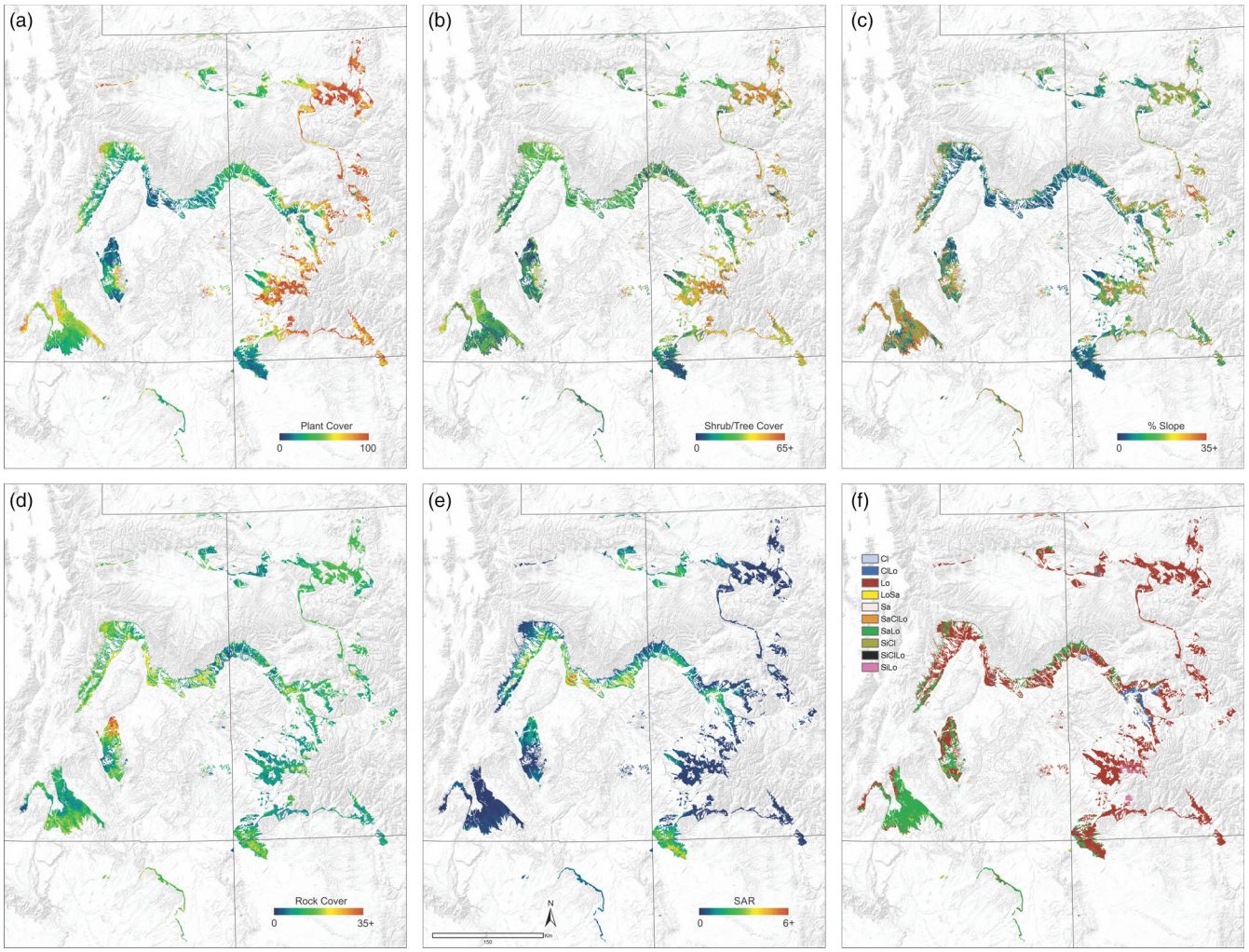

FIGURE 3 Geospatial variables: (a) plant cover, (b) shrub cover, (c) slope, (d) rock cover, (e) SAR, and (f) soil texture [Colour figure can be viewed at wileyonlinelibrary.com]

artifacts in digital elevation models, often producing stepped changes in value. In order to minimize this effect, the 10-m data were smoothed using a 9×9 Gaussian low-pass filter (Milledge, Lane, & Warburton, 2009; Walker & Willgoose, 1999) and then resampled to the 30-m resolution of the other raster datasets prior to calculating slope. This smoothing would be expected to have a minimal effect on 30-m slope estimates while ameliorating data artifacts. The RHEM model characterizes slope using sine of the slope angle, which at low slope values is similar to percent slope. In order to provide information on slope shape for RHEM, the longitudinal convexity of the smoothed 30-m DEM was calculated using the topographic modeling function in the ENVI image processing software package (Version 5.5, Harris Geospatial). Based on visual interpretation of the slope and elevation datasets, a longitudinal convexity less than −0.25 was labeled convex, convexity up to 0.25 was labeled 'uniform,' and values beyond 0.25 were concave.

High-resolution SSURGO digital soils data from NRCS is not available for large portions of the Mancos Shale, and the lower resolution NRCS STATSGO soil maps are not sufficiently detailed for this scale of modeling. However, Nauman et al. (2019) used statistical models to develop uninterrupted estimates of soil parameters for the UCRB at a 30-m grid resolution. Percentages of sand, silt, and clay from Nauman et al. were converted to the 12 USDA soil texture classes for RHEM (Figure 3f) using the soiltexture package (Moeys et al., 2018) that is available for the R statistical software package (R Core Team, 2018). Maps of statistically estimated rock fragment size, rock cover, and sodium adsorption ratio (SAR, Figure 3e) also were taken from Nauman et al. (2019). For RHEM, rock cover was set to 0% if the estimated fragment size was less than 5 mm, and the estimated total rock cover was applied to the remaining areas (Figure 3d).

The precipitation rates used in this study were taken from the gridded datasets of Atlas 14 of the United States National Atmospheric and Oceanographic Administration (NOAA). The RHEM model was run using 30- and 60-min duration storms associated with 10- and 25-year return intervals (four simulations). The study area overlapped two different geographic regions of the Atlas 14 product, Midwest and Southwest, and there were noticeable discrepancies along the boundaries of these two regions. This issue is considered later in the interpretation of model outputs.

The rangeland hydrology and erosion model includes a term for canopy water storage that absorbs an initial quantity of rainfall. An accurate determination of this value is difficult, since interception and storage depend on canopy geometry, leaf angle distribution, type of foliage, and characteristics of precipitation and wind speed (Dunkerley, 2008; Owens, Lyons, & Alejandro, 2006; Pierson & Williams, 2016). However, this static storage term is generally small compared to the totals of larger rainfall events, such as those tested in this study. The MCD15A3H product that is generated from NASA's MODIS sensor system on the Terra and Aqua satellites provides an estimate of leaf area index (LAI) that is based on general vegetation type and land surface reflectance. This LAI measure is the ratio of one-sided leaf area to ground area. The LAI product is produced at a 500-m spatial resolution and was resampled to 30 m using bilinear interpolation. Based loosely on Breuer, Eckhardt, and Frede (2003), we assumed that the canopy stored 0.4*LAI mm of precipitation.

Per-pixel inputs and outputs of the RHEM model were managed using the IDL software package (version 8.7, Harris Geospatial). This study used version 2.3 of the command line version of the RHEM model, with the addition of the SAR parameter developed in Nouwakpo et al. (2018). The command line version of RHEM provides more control of model parameters than the web-based version that is available on the internet. The four modeled storm events were sampled with a 15 s time step, which was dynamically altered by RHEM as required for numerical stability. In order to reduce processing time for the more than 22 million Mancos Shale pixels, floating point input parameters were binned to discrete values, and the results for unique combinations of binned input values were stored for future use instead of re-running the model. This discretization balanced the expected sensitivity of model parameters with the relative precision of input data sources. Slope was binned to percents (e.g., 0–1% = 0.5%). Total vegetation cover and shrub cover were binned by 5% intervals, and LAI to 0.25 intervals. Total rainfall was binned to 2.54 mm (0.1 in.) increments. SAR was binned to unit intervals (maximum SAR pixel value = 18).

Prior studies have performed rainfall experiments with the Walnut Gulch Rainfall Simulator (WGRS) at sites on the Mancos shale and nearby saline outcrops (Cadaret, McGwire, et al., 2016; Cadaret, Nouwakpo, et al., 2016; Nouwakpo et al., 2018), and those data were used to assess the performance of this regional RHEM modeling approach. Specific GPS coordinates for each WGRS plot were not available, but map polygons indicating the spatial extent of each field site allowed average GIS parameters to be calculated. The field site names and their geographic centroids are identified in Table 1. Multiple WGRS experiments were performed at each of these field sites, using a range of rainfall intensities from 50.8 to 139.7 mm/hr. The cumulative sediment yields after 20 min of WGRS rainfall were averaged for each intensity setting at each site and correlated with the 20-min GIS-driven RHEM estimate for these locations and intensities.

3 | RESULTS

The time required to run RHEM for the entire Mancos Shale study area ranged from 29.4 to 49.4 hr on a PC with a 3.4 GHz I7-4770 processor, with the larger range of precipitation values in the 25-year 60-min storm creating the greatest number of unique permutations of input parameters and time. Sediment yield estimates (t/ha) from the four storm simulations were highly correlated, so only the result for the 25-year 60-min simulation is presented in Figure 4. The full output resolution could not be rendered directly, so the data in that figure were averaged to a 1 ha resolution. Table 2 lists the mean and maximum sediment yields associated with each storm simulation. There was an approximate doubling of mean estimated yields between the 10- and 25-year storms, but more than 15-fold increase from 30- to 60-min storms. This reflects the greater relative effect of canopy interception and initial infiltration on shorter storms.

TABLE 1 Walnut Gulch rainfall simulator site names, geological formations, and geographic centroids (UTM zone 12, NAD83)

Site name	State	Formation	Easting	Northing
Delta	Colorado	Mancos Shale	758,564	4,298,777
Ferron	Utah	Mancos Shale	489,389	4,313,805
Ferron2H	Utah	Mancos Shale	489,441	4,313,888
Ferron2L	Utah	Mancos Shale	489,641	4,313,859
Ferron2M	Utah	Mancos Shale	489,740	4,314,389
Farmington	New Mexico	Nacimiento	774,513	4,051,428
Loma	Colorado	Mancos Shale	682,411	4,358,501
Moab	Utah	Mancos Shale	598,146	4,295,795
Moab2	Utah	Mancos Shale	595,796	4,295,259
Price	Utah	Mancos Shale	533,766	4,368,225
Rangely	Colorado	Mancos Shale	683,914	4,449,664

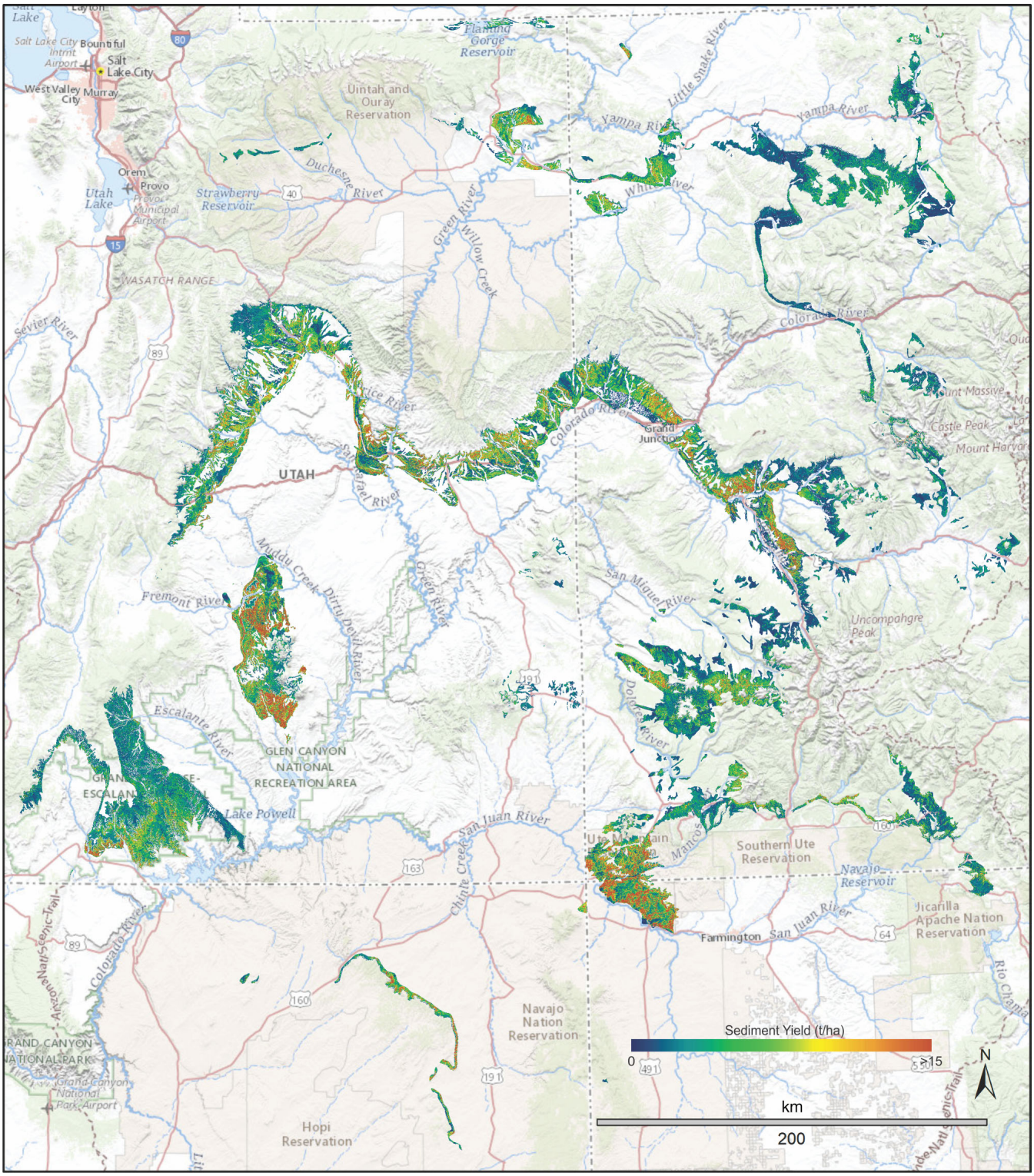

FIGURE 4 Sediment yield (t/ha) for 25-year, 60-min storm (terrain reference: USGS National Map) [Colour figure can be viewed at wileyonlinelibrary.com]

Figure 5 plots the log of sediment yield versus selected model inputs for more than 8,000 randomly selected points within the study area, and it provides the corresponding Spearman's rank-order correlations (ρ). The results show that sediment yield is a complex function of the input variables, with no single variable explaining the majority of variance. Differences in rainfall rates across the region have little predictive value. As expected, yield increases with slope and SAR, but a relatively large proportion of samples maintain lower yields despite

high values in either parameter. Conversely, yield is negatively related to total vegetation cover, but there are locations that are predicted to have relatively high yields despite high vegetation cover.

Figure 6 presents the distribution of values for sediment yield and several input variables for each soil type. The greatest sediment yields were associated with silt loam soils, which are often prone to erosion since silt particles do not form aggregates and are easily mobilized (Wischmeier & Mannering, 1969). Compounding this, the silt loams in the study area are mapped as occurring in compact areas that happen to have the highest precipitation and greatest average slope (Figure 6b,c). These soils are largely responsible for the unexpectedly high yields in locations with high vegetation cover (Figure 6d) that are seen in Figure 5c.

Figure 7 compares cumulative sediment yield after 20 min from the WGRS experiments (Table 1) and the corresponding duration for these locations using the RHEM model with geospatial inputs. Figure 7a illustrates that the model greatly under-predicted erosion at the Ferron locations, and that the distribution of variance was generally non-normal for both the WGRS experiments and the RHEM predictions. Given the non-normal distribution, Spearman's rank-order correlation was used, and the nonparametric correlation between the model and the rainfall experiments was .760, even when including the Ferron sites. Figure 7b shows the rank-ordered relationship between RHEM and WGRS. Figure 7c shows rank-orders for a test where RHEM used field-measured SAR data from Ferron taken from Cadaret, Nouwakpo, et al. (2016) instead of the mapped values.

TABLE 2 Rangeland hydrology and erosion model sediment yields (t/ha)

Storm	Mean	Maximum
10-year 30-min	0.18	24.8
10-year 60-min	3.12	237.6
25-year 30-min	0.36	36.4
25-year 60-min	5.58	366.7

4 | DISCUSSION

Weltz et al. (2014) characterized erosion potential on nonfederal rangelands across the western United States using field data from NRI and RHEM. However, using map data from the Protected Areas Database (USGS, 2018) and the US Forest Service, Table 3 indicates that the majority of the Mancos Shale study area is managed by federal agencies. Note that areas of high urban or agricultural development or slopes greater than 35% were removed from the calculations in Table 3. Based on Weltz et al. (2014), RHEM output for the 25-year, 60-min storm was categorized as low risk (< 2 t/ha), medium risk (2–4 t/ha) or high risk (>4 t/ha), and the area in each category is presented in Table 3. The Bureau of Land Management manages the majority of rangelands on the Mancos Shale, and it also has the greatest area with erosion rates in excess of 4 t/ha. Private lands cover 27% of the Mancos Shale study area, but contained

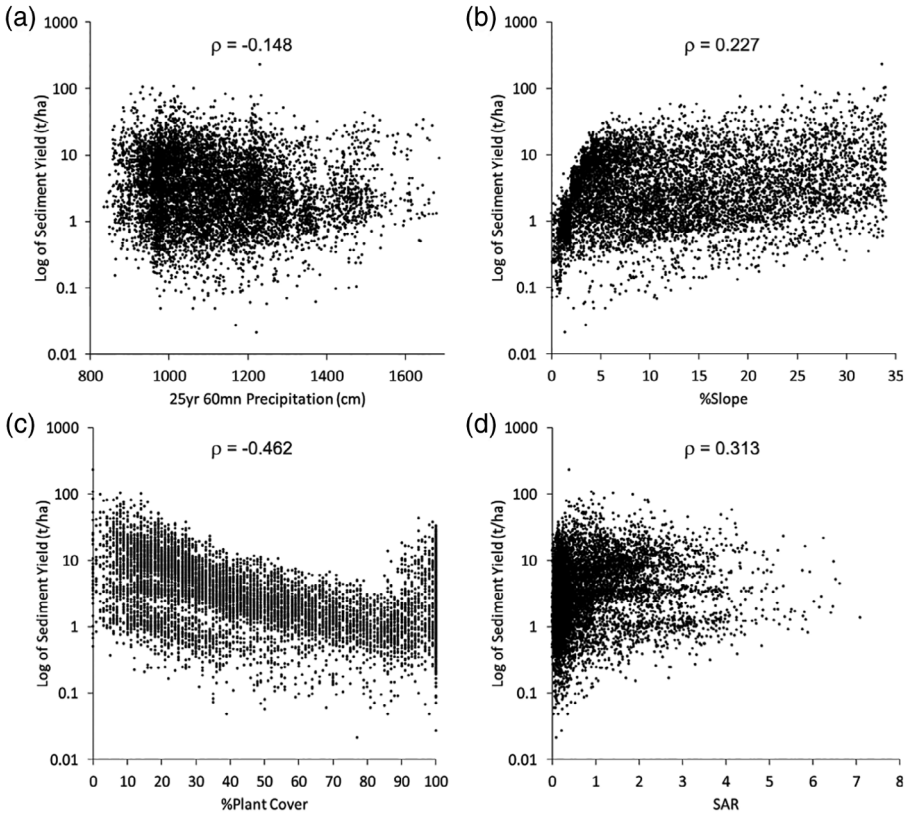

FIGURE 5 Log sediment yield versus (a) precipitation amount, (b) percent slope, (c) percent vegetation cover, and (d) sodium adsorption ratio with Spearman's rho

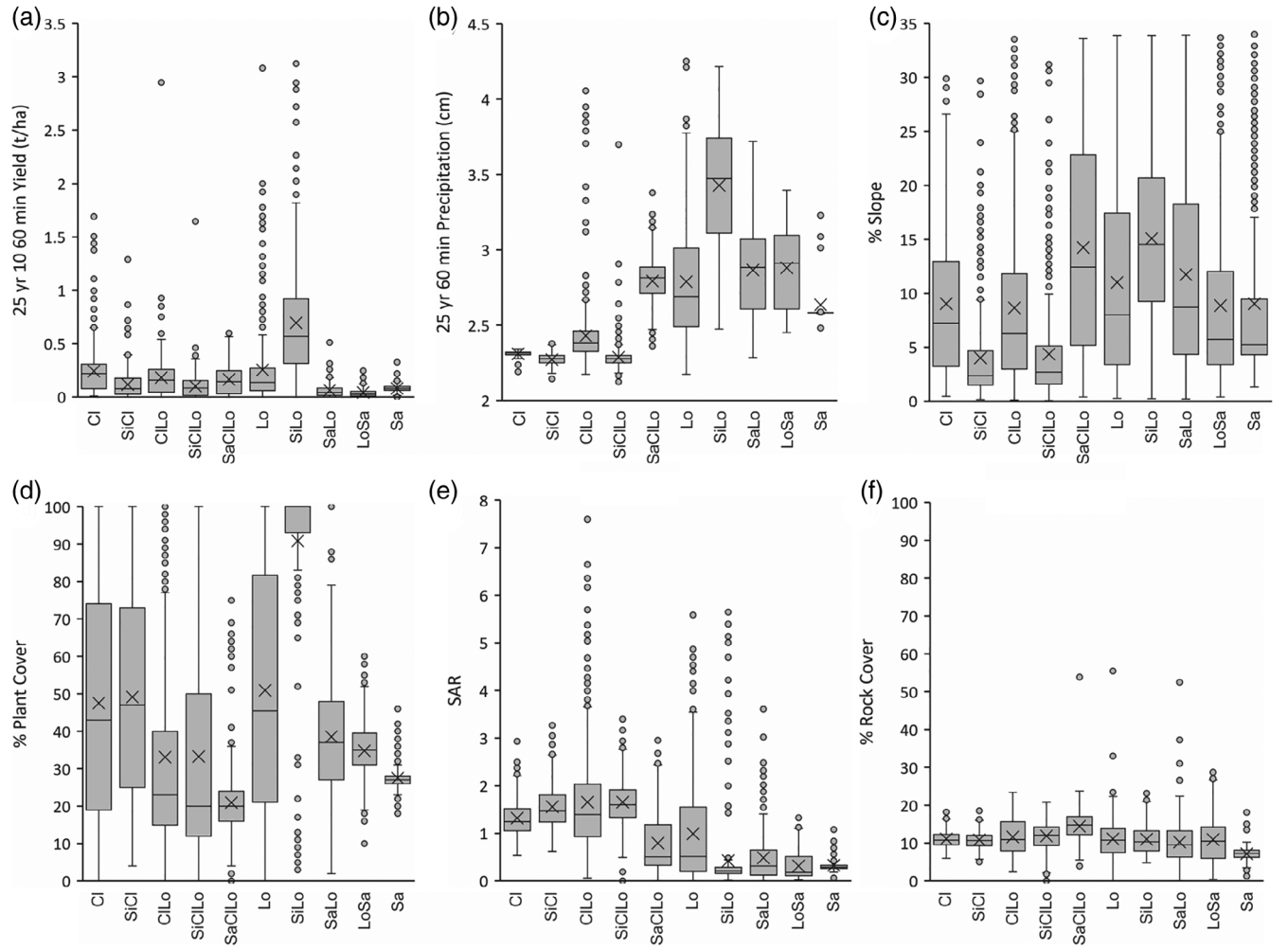

FIGURE 6 Relationship of soil texture to (a) sediment yield, (b) precipitation, (c) percent slope, (d) percent vegetation cover, (e) sodium adsorption ratio, and (f) percent rock cover

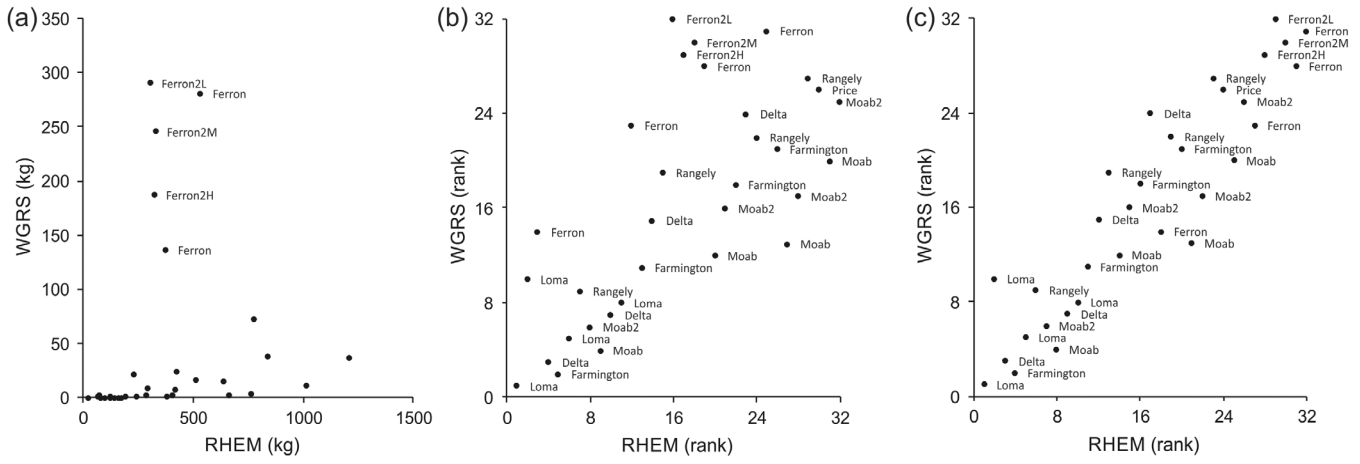

FIGURE 7 Erosion from the rangeland hydrology erosion model versus Walnut Gulch rainfall simulator experiments (a: sediment yield, b: rank order, c: rank order using field-measured sodium adsorption ratio for Ferron sites).

TABLE 3 Area of the Mancos Shale study area by land management category and erosion risk (low <2 t/ha, medium 2–4 t/ha, high >4 t/ha), sorted by area at high risk

Management	Total (ha)	Low risk (ha)	Medium risk (ha)	High risk (ha)	High risk (%)
US Bureau of Land Management	789,463	218,025	196,825	374,613	47.5
Private	471,659	274,991	93,242	103,426	21.9
Tribes	145,886	30,523	26,611	88,752	60.8
US Forest Service	229,009	117,957	47,216	63,836	27.9
State Lands	112,851	39,795	27,343	45,713	40.5
US Bureau of Reclamation	831	229	219	383	46.1
US Fish and Wildlife Service	17	8	7	2	11.8

proportionately less area of high erosion risk, possibly reflecting the negative economic impacts of salinity and soil erosion on decision making regarding private land ownership. Given that urbanized and agricultural areas were removed from this study, the actual area of private ownership on the entire Mancos Shale is larger than that reported in Table 3. Also, since irrigated agriculture on the Mancos Shale is potentially a dominant salinity source (Tuttle et al., 2014), the actual percentage of private lands at high risk would depend on the areal proportion of irrigated agriculture. Future efforts could composite this RHEM product with map-based agricultural salinity estimates to provide better regional information. Tribal lands cover only 8% of the total study area, but they generally have low levels of vegetation cover and the majority of their area was classified as high risk. Conversely, Forest Service lands tend to have high vegetation cover, and therefore have a lower percentage of land at high risk than the other public agencies with large land holdings.

The RHEM model provides a hillslope-scale estimate of soil erosion risk, so the risk map in Figure 4 does not account for streambank erosion, gullying, or transport and deposition at a broader scale. However, it does provide a useful representation of which areas would be expected to be most in need of soil conservation efforts. Figure 6 indicates that the area of greatest erosion risk is on steeper slopes with silt loam soils, despite the fact that these sites are generally well vegetated. However, these figures do not communicate the great difference in the spatial extent of different soil textures, and that only slopes less than 35% were considered. The mapped extent of silty loam was just 1.7% of the study area, while loam covered 40 times more area. Thus, while other soils had areas with high values for yield, precipitation, slope, and cover, their overall statistical distribution trended lower than the small regions of silt loam in Figure 6.

In assessing the uncertainty of the model outputs, there are numerous issues of scale when attempting to relate the GIS-driven RHEM model (900 m^2 pixels) to the WGRS experiments (12 m^2 plots). Site selections for the prior WGRS studies were made to target specific types of slope and vegetation cover, rather than attempting to provide an unbiased representation of the wider environment. Conversely, generalization in the creation of map data means that plot-level heterogeneity could not be represented in RHEM. Also, each map input has some level of measurement or attribute error. The differences between RHEM and WGRS erosion estimates at the Ferron locations (Figure 7a) are primarily due to a map error. Cadaret, Nouwakpo, et al. (2016) report an extraordinarily high laboratory-measured SAR value of 35.2 for the Ferron location, while the statistically modeled map estimate from Nauman et al. (2019) predicted an average value of 1.24 for these sites. This is important, since a high SAR creates very dispersive and erodible soil. Substituting the SAR value reported by Cadaret, Nouwakpo, et al. (2016) for Ferron locations, Spearman's rank-order correlation between RHEM and the WGRS simulations increased to .926 (Figure 7c), indicating a very strong predictive relationship for mapping relative erosion risk with RHEM when the GIS inputs are accurate. The relative importance of the uncertainty in the SAR map may be lower if an area has high predicted sediment yield despite low SAR inputs, or vice versa. For example, the area of very high SAR values in Figure 3e (orange, left of center) has relatively low sediment yield in Figure 4, due primarily to very low slopes (Figure 3c) and moderate rock cover (Figure 3d). In that case, we might presume that the uncertainty in those high SAR values is less an issue than for an area of moderate or steep slopes where the predicted SAR and yield are both low. Also, one could identify discrepancies between the RHEM SAR input or predicted yield versus prior studies of stream chemistry like Tillman et al. (2018). Since we used datasets from Nauman et al. (2019), that source should not be considered independent. Beyond the specific case of SAR, many soil properties across the Mancos Shale are the result of heterogenous, fine-scale deposition processes (Tuttle et al., 2014) that cannot be mapped with commensurate precision.

Another issue with the accuracy of RHEM inputs was apparent with discrepancies along the boundary between regional precipitation products from NOAA Atlas 14. Little of this boundary zone intersected the Mancos Shale, and the output from the RHEM model does not show a very dramatic visible difference. The average difference in precipitation across this boundary where the Mancos Shale was present was about 3 mm for the 25-year 60-min data. The largest local discontinuity is north of Shiprock, New Mexico, but the effect on predicted yields appeared weak in a visual inspection of the RHEM output. There is potential for improving a future version of Atlas 14 by increasing the amount of overlap between regions during the interpolation, and by deriving interpolation parameters in a more localized manner. However, in this study the uncertainty in

the SAR map product was likely much more of an issue than the precipitation.

While this study did not include biological soil crusts due to the lack of a known map data source, they are an important component of most ecosystems in the study area and can have important effects on soil erosion (Carpenter & Chong, 2010; Belnap, 2006; Gao, Bowker, Sun, Zhao, & Zhao, 2020). The greatest amount of biocrust at the WGRS field sites was an average of 53% cover at Delta. Even though the soil crust parameter was not used in RHEM, data points associated with the Delta site are not outliers in Figure 7b,c. This is interesting, given that a RHEM-based analysis by Fick, Belnap, and Duniway (2020) found that soil crusts were the most effective variable for explaining erosion differences between paired Mancos Shale watersheds that had different grazing histories. The contrasting finding of Fick et al. may be due to the comparable nature of their paired environments, whereas the wide range of slopes, soil types, and vegetation cover that is modeled here surpasses the variability in erosion rates due to crusts. It will be important for decision makers to acknowledge the possible role of soil crusts when using this RHEM map to prioritize various sites for study or erosion control activities.

Rangeland hydrology and erosion model predictions of relatively high sediment yield on silt loams with high vegetation cover (Figure 5c) are important for interpreting studies like Nauman et al. (2019) that limit expected sediment and salinity source areas to very bare soils. Regardless of what is driving RHEM, many studies (Pierson et al., 2010, 2013; Roundy et al., 2017; Williams et al., 2014) document that encroachment of dense pinyon-juniper tree cover in the arid southwest can lead to greatly increased soil erosion as intervening herbaceous cover is suppressed and concentrated flow paths in the interspaces come to dominate surface flow.

Background soil color is known to affect satellite-based vegetation indices in areas with limited vegetation cover (Huete & Tucker, 1991). Kautz et al. (2019) also used a Landsat vegetation index to predict foliar cover for the RHEM model, obtaining a very high R^2 of .85 for predicting cover. However, that study was for a single, small watershed with fewer confounding effects than the broad scale of application performed here. Using 134 NRI points spread across the region, our regression between NDVI and foliar cover had a good, but lower, R^2 of .70. The strong relationship between RHEM and the WGRS experiments after correcting the known SAR error (Figure 7c) suggests that LANDSAT-based estimates of vegetation cover are a useful input for process-based models of soil erosion at this scale of application, despite the influence of soil color.

An issue not dealt with in this study is temporal variation in landscape characteristics. At a fine scale, the seasonal leafing-out of vegetation makes foliar cover and canopy storage parameters dependent on the date of a given storm. This concern is ameliorated to some degree by the circumstance that the most intense precipitation in the region is typically associated with late summer monsoonal events when much of the potential leaf area would have been developed. However, herbivory could reduce leaf area through a season, counteracting this assumption in our method. Also, making litter cover a simple function of total vegetation cover does not consider that the generation and removal of plant litter varies through a season, and it depends greatly on the types of vegetation and land management. Also at a seasonal time scale, RHEM only predicts erosion from rainfall events, so contributions of sediment and salinity associated with snowmelt are not considered in this analysis. Long-term patterns of land use and grazing create spatially dependent variability in soil and vegetation characteristics (Duniway, Geiger, Minnick, Phillips, & Belnap, 2018) that are not reflected in our map and image inputs. Plant succession, sporadic wildfires, and dramatic disturbance events in the region eventually will render the current RHEM inputs obsolete in some locations.

Despite the many uncertainties in map inputs and the fact that the WGRS field experiments were not designed for the purpose of model validation, the high rank-order correlation between RHEM and WGRS simulations indicates that the RHEM product can provide useful insights for prioritization of locations where rangeland soil erosion is most likely to affect water quality. Given the nature of errors in various map inputs, field observations will be important for decision making that incorporates this RHEM product.

5 | CONCLUSIONS

This study demonstrated the ability to apply the process-based RHEM model of soil erosion over a large geographic domain for the purpose of assessing relative levels of risk to water quality. In particular, the focus on saline soils of the Mancos Shale and previously documented correlations between sediment yield and salinity on these formations can provide insights into sources of salinity to the Colorado River.

Given the uncertainties of map accuracy and differences of scale in comparing WGRS simulations to the GIS-driven RHEM model, the moderately strong Spearman's correlation of .76 between the RHEM model and independent field studies provides good confidence in using the results as a starting point for decision making. However, the example of incorrect specification for SAR at the Ferron sites highlights the importance of incorporating other available sources of information and expertise.

Because they are based on physical properties of the soil and the specific growth forms of plant cover, physical models like RHEM are more defensible than USLE-based empirical methods when exploring the implications of alternative scenarios for rainfall regimes and changes in land cover or management. The application of RHEM at a per-pixel level is shown to provide a useful way to characterize hillslope-scale erosion over a very large region, identifying specific high-risk areas for mitigation methods like micro-catchments (Founds, McGwire, Weltz, & Verburg, 2020), or for localized implementation of more sophisticated, time-consuming models like WEPP (Flanagan, Ascough, Nearing, & Laflen, 2001) or KINEROS2 (Smith, Goodrich, & Quinton, 1995) that consider flow routing and deposition across a watershed. The erodible, saline soils of the Mancos Shale contain areas of high erosion risk across federal, state, and private lands, and this high-resolution map of predicted

erosion can help those stakeholders to implement more effective soil conservation efforts for improving water quality of the Colorado River.

Results for the 60-min, 25-year storm simulation are available as a GeoTIFF through the USDA National Agricultural Library at https://doi.org/10.15482/USDA.ADC/1518465.

ACKNOWLEDGMENTS

This research was supported by a Cooperative Agreement 59-2060-6-001 with the Agricultural Research Service of the U.S. Department of Agriculture that is in turn funded through Agreement 60-5370-4-001 from the US Bureau of Land Management.

CONFLICT OF INTEREST

Dr. McGwire certifies that he has received verification from all co-authors that there are no potential conflicts of interest associated with the research presented herein.

ORCID


Kenneth C. McGwire https://orcid.org/0000-0002-4751-8072

REFERENCES

Belnap, J. (2006). The potential roles of biological soil crusts in dryland hydrologic cycles. *Hydrological Processes*, *20*, 3159–3178. https://doi.org/10.1002/hyp.6325

Breuer, L., Eckhardt, K., & Frede, H.-G. (2003). Plant parameter values for models in temperate climates. *Ecological Modelling*, *169*, 237–293. https://doi.org/10.1016/s0304-3800(03)00274-6

Cadaret, E. M., McGwire, K. C., Nouwakpo, S. K., Weltz, M. A., & Saito, L. (2016). Vegetation canopy cover effects on sediment erosion processes in the upper Colorado River basin Mancos Shale formation, Price, Utah, USA. *Catena*, *147*, 334–344. https://doi.org/10.1016/j.catena.2016.06.043

Cadaret, E. M., Nouwakpo, S. K., McGwire, K. C., Weltz, M. A., & Blank, R. R. (2016). Experimental investigation of the effect of vegetation on soil, sediment erosion, and salt transport processes in the upper Colorado River basin Mancos Shale formation, Price, Utah, USA. *Catena*, *147*, 650–662. https://doi.org/10.1016/j.catena.2016.08.024

Carpenter, D. R., & Chong, G. W. (2010). Patterns in the aggregate stability of Mancos Shale-derived soils. *Catena*, *80*, 65e73. https://doi.org/10.1016/j.catena.2009.09.001

Curran, P., & Hay, A. (1986). The importance of measurement error for certain procedures in remote sensing at optical wavelengths. *Photogrammetric Engineering and Remote Sensing*, *52*, 299–241.

Duniway, M. C., Geiger, E. L., Minnick, T. J., Phillips, S. L., & Belnap, J. (2018). Insights from long-term Ungrazed and grazed watersheds in a Salt Desert Colorado plateau ecosystem. *Rangeland Ecology & Management*, *71*, 492–505. https://doi.org/10.1016/j.rama.2018.02.007

Dunkerley, D. (2008). Intra-storm evaporation as a component of canopy interception loss in dryland shrubs: Observations from Fowlers Gap, Australia. *Hydrological Processes*, *22*, 1985–1995. https://doi.org/10.1002/hyp.6783

Fick, S. E., Belnap, J., & Duniway, M. C. (2020). Grazing-induced changes to biological soil crust cover mediate hillslope erosion in long-term Exclosure experiment. *Rangeland Ecology & Management*, *73*, 61–72. https://doi.org/10.1016/j.rama.2019.08.007

Flanagan, D. C., Ascough, J. C., Nearing, M. A., & Laflen, J. M. (2001). The water erosion prediction project (WEPP) model. In R. S. Harmon & W. W. Doe (Eds.), *Landscape erosion and evolution modeling*. Boston, MA: Springer. https://doi.org/10.1007/978-1-4615-0575-4_7

Founds, M., McGwire, K. C., Weltz, M. A., & Verburg, P. S. J. (2020). Predicting micro-catchment infiltration dynamics. *Catena*, *190*, 104524. https://doi.org/10.1016/j.catena.2020.104524

Gao, L. Q., Bowker, M. A., Sun, H., Zhao, J., & Zhao, Y. G. (2020). Linkages between biocrust development and water erosion and implications for erosion model implementation. *Geoderma*, *357*, 113973. https://doi.org/10.1016/j.geoderma.2019.113973

Hernandez, M., Nearing, M. A., Stone, J. J., Pierson, F. B., Wei, H., Spaeth, K. E., … Goodrich, D. C. (2013). Application of a rangeland soil erosion model using National Resources Inventory data in southeastern Arizona. *Journal of Soil and Water Conservation*, *68*, 512–525. https://doi.org/10.2489/jswc.68.6.512

Huntington, J., McGwire, K., Morton, C., Snyder, K., Peterson, S., Erickson, T., … Allen, R. (2016). Assessing the role of climate and resource management on groundwater dependent ecosystem changes in arid environments with the Landsat archive. *Remote Sensing of Environment*, *185*, 186–197. https://doi.org/10.1016/j.rse.2016.07.004

Huete, A. R., & Tucker, C. J. (1991). Investigation of soil influences in AVHRR red and near-infrared vegetation index imagery. *International Journal of Remote Sensing*, *12*, 1223–1242. https://doi.org/10.1080/01431169108929723

Iorns, W. V., Hembree, C. H, & Oakland, G. L. (1965). Water resources of the upper Colorado River basin. Technical report: U.S. Geological Survey Professional Paper 441, 370 p.

Kautz, M. A., Holifield-Collins, C. D., Guertin, D. P., Goodrich, D. C., van Leeuwen, W. J., & Williams, C. J. (2019). Hydrologic model parameterization using dynamic LANDSAT-based vegetative estimates within a semiarid grassland. *Journal of Hydrology*, *575*, 1073–1086. https://doi.org/10.1016/j.jhydrol.2019.05.044

Kenney, T. A., Gerner, S. J., Buto, S. G., & Spangler, L. E. (2009). Spatially referenced statistical assessment of dissolved-solids load sources and transport in streams of the upper Colorado River basin. USGS Scientific Investigations Report, U.S. Geological Survey, Reston, Virginia. 50 p.

Kinnell, P. I. A. (2005). Why the universal soil loss equation and the revised version of it do not predict event erosion well. *Hydrological Processes*, *19*, 851–854. https://doi.org/10.1002/hyp.5816

McGwire, K., Friedl, M., & Estes, J. (1993). Spatial structure, sampling design, and scale in remotely sensed imagery of a California savanna woodland. *International Journal of Remote Sensing*, *14*, 2137–2164. https://doi.org/10.1080/01431169308954026

Milledge, D. G., Lane, S. N., & Warburton, J. (2009). The potential of digital filtering of generic topographic data for geomorphological research. *Earth Surface Processes and Landforms*, *34*, 63–74. https://doi.org/10.1002/esp.1691

Miller, M. P., Buto, S. G., Lambert, P. M., & Rumsey, C. A. (2017). Enhanced and updated spatially referenced statistical assessment of dissolved-solids load sources and transport in streams of the upper Colorado River basin. U.S. Geological Survey Scientific Investigations Report 2017–5009, 23 p.

Moeys, J., Shangguan, W., Petzold, R., Minasny, B., Rosca, B., Jelinski, N., … ten Caten, A. (2018). Functions for Soil Texture Plot, Classification and Transformation (version 1.5.1). Retrieved from https://github.com/julienmoeys/soiltexture

Nauman, T. W., Ely, C. P., Miller, M. P., & Duniway, M. C. (2019). Salinity yield modeling of the upper Colorado River basin using 30-meter resolution soil maps and random forests. *Water Resources Research*, *55*, 4954–4973. https://doi.org/10.1029/2018WR024054

Nearing, M. A., Wei, H., Stone, J. J., Pierson, F. B., Spaeth, K. E., Weltz, M. A., … Hernandez, M. (2011). A rangeland hydrology and erosion model. *Transactions of the ASABE*, *54*, 901–908. https://doi.org/10.13031/2013.37115

Nouwakpo, S. K., Weltz, M. A., Arslan, A., Green, C. H., & Al-Hamdan, O. Z. (2018). Process-based modeling of infiltration, soil loss, and dissolved

solids on saline and sodic soils. *Transactions of the ASABE*, *61*, 1033–1048. https://doi.org/10.13031/trans.12705

Owens, M. K., Lyons, R. K., & Alejandro, C. L. (2006). Rainfall partitioning within semiarid juniper communities: Effects of event size and canopy cover. *Hydrological Processes*, *20*, 3179–3189. https://doi.org/10.1002/hyp.6326

Pierson, F. B., & Williams, C. J. (2016). Ecohydrologic impacts of rangeland fire on runoff and erosion: A literature synthesis. Fort Collins: U. S. Dept of Agriculture, Forest Service, Rocky Mountain Research Station.

Pierson, F. B., Williams, C. J., Kormos, P. R., Hardegree, S. P., Clark, P. E., & Rau, B. M. (2010). Hydrologic vulnerability of sagebrush steppe following pinyon and juniper encroachment. *Rangeland Ecology & Management*, *63*, 614–629. https://doi.org/10.2111/rem-d-09-00148.1

Pierson, F. B., Williams, C. J., Hardegree, S. P., Clark, P. E., Kormos, P. R., & Al-Hamdan, O. Z. (2013). Hydrologic and erosion responses of sagebrush steppe following juniper encroachment, wildfire, and tree cutting. *Rangeland Ecology & Management*, *66*, 274–289. https://doi.org/10.2111/rem-d-12-00104.1

R Core Team (2018). R: A language and environment for statistical computing. Vienna, Austria: R Foundation for Statistical Computing. https://www.R-project.org/

Roundy, B. A., Farmer, M., Olson, J., Petersen, S., Nelson, D. R., Davis, J., & Vernon, J. (2017). Runoff and sediment response to tree control and seeding on a high soil erosion potential site in Utah: Evidence for reversal of an abiotic threshold. *Ecohydrology*, *10*, e1775. https://doi.org/10.1002/eco.1775

Rouse, J. W., Haas, R. H., Schell, J. A., Deering, D. W., & Harlan, J. C. (1974). Monitoring the vernal advancement and retrogradation (greenwave effect) of natural vegetation. NASA/GSFC Type III Final Report, Greenbelt.

Shirnian-Orlando, A. A., & Uchrin, C. G. (2000). A method for determining salt sources in surface waters. *Journal of the American Water Resources Association*, *36*, 749–757. https://doi.org/10.1111/j.1752-1688.2000.tb04303.x

Smith, R. E., Goodrich, D. C., & Quinton, J. N. (1995). Dynamic, distributed simulation of watershed erosion: The KINEROS2 and EUROSEM models. *Journal of Soil and Water Conservation*, *50*, 517–520.

Spaeth, K. E., Pierson, F. B., Weltz, M. A., & Blackburn, W. H. (2003). Evaluation of USLE and RUSLE estimated soil loss on rangelands. *J. Range Management*, *56*, 234–246. https://doi.org/10.2458/azu_jrm_v56i3_spaeth

Spaeth, K. E., Pierson, F. B., Herrick, J. E., Shaver, P. L., Pyke, D. A., Pellant, M., … Dayton, B. (2003). New proposed national resources inventory protocols on nonfederal rangelands. *Journal of Soil and Water Conservation*, *58*, 18A–21A.

Spahr, N.E., Apodaca, L.E., Deacon, J.R., Bails, J.B., Bauch, N.J., Smith, M., & Driver, N.E. (2000). Water quality in the upper Colorado River basin, Colorado, 1996–98. U.S. Geological Survey Circular 1214. Denver, CO.

Tillman, F. D., Anning, D. W., Heilman, J. A., Buto, S. G., & Miller, M. P. (2018). Managing salinity in upper Colorado River basin streams: Selecting catchments for sediment control efforts using watershed characteristics and random forests models. *Water*, *10*, 676. https://doi.org/10.3390/w10060676

Toney, C., Shaw, J. D., & Nelson, M. D. (2009). A stem-map model for predicting tree canopy cover of forest inventory and analysis (FIA) plots. Forest Inventory and Analysis (FIA) Symposium October 21-23, 2008, Proceedings RMRS-P-56, Rocky Mountain Research Station. Fort Collins, CO.

Tuttle, M. L., Fahy, J. W., Elliott, J. G., Grauch, R. I., & Stillings, L. L. (2014). Contaminants from cretaceous black shale: II. Effect of geology, weathering, climate, and land use on salinity and selenium cycling, Mancos Shale landscapes, southwestern United States. *Applied Geochemistry*, *46*, 72e84. https://doi.org/10.1016/j.apgeochem.2013.12.011

NRCS (U.S. Department of Agriculture National Resource Conservation Service) (1997). National resources inventory. Natural Resources Conservation Service. Revised 2014.

NRCS (U.S. Department of Agriculture National Resource Conservation Service) (2018). 2018 National Resources Inventory Rangeland Resource Assessment. Retrieved from https://www.nrcs.usda.gov/wps/portal/nrcs/detail/national/technical/nra/nri/results/?cid=nrcseprd1343027

USBOR (U.S. Bureau of Reclamation). (2013). Quality of water—Colorado River basin progress report No. 24. USBOR Upper Colorado Region, Salt Lake City, UT.

USGS (U.S. Geological Survey). (2002). National elevation dataset, 1/3 arc second. Retrieved from http://ned.usgs.gov

USGS (U.S. Geological Survey). (2017). LANDFIRE 1.4.0. Retrieved from https://www.LANDFIRE.gov

USGS (U.S. Geological Survey) (2018). Protected Areas Database of the United States (PAD-US). Retrieved from https://usgs.gov/gapanalysis/PAD-US

Walker, J. P., & Willgoose, G. R. (1999). On the effect of digital elevation model accuracy on hydrology and geomorphology. *Water Resources Research*, *35*, 2259–2268. https://doi.org/10.1029/1999wr900034

Warner, J. W., Heimes, F. J., & Middelburg, R. F. (1985). Ground-water contribution to the salinity of the upper Colorado River basin. USGS Water-Resources Investigations Report, U.S. Geological Survey. p. 113.

Weltz, M. A., Kidwell, M. R., & Fox, D. H. (1998). Influence of abiotic and biotic factors in measuring and modeling soil erosion on rangelands: State of knowledge. *Journal of Range Management*, *51*, 482–495. https://doi.org/10.2307/4003363

Weltz, M. A., Jolley, L., Hernandez, M., Spaeth, K. E., Rossi, C., Talbot, C., … Morris, C. (2014). Estimating conservation needs for rangelands using national inventory assessments. *American Society of Agricultural and Biological Engineers*, *57*, 1559–1570. https://doi.org/10.13031/trans.57.10030

Williams, C. J., Pierson, F. B., Al-Hamdan, O. Z., Kormos, P. R., Hardegree, S. P., & Clark, P. E. (2014). Can wildfire serve as an ecohydrologic threshold reversal mechanism on juniper- encroached shrublands? *Ecohydrology*, *7*, 453–477. https://doi.org/10.1002/eco.1364

Wischmeier, W. H., & Mannering, J. V. (1969). Relation of soil properties to its erodibility. *Soil Science Society of America Journal*, *33*, 131–137. https://doi.org/10.2136/sssaj1969.03615995003300010035x

Wischmeier, W. H., & Smith, D. D. (1978). Predicting rainfall-erosion losses: A guide to conservation planning. Agriculture Handbook (AH) 537. U.S. Dept. of Agriculture, Washington, DC.

How to cite this article: McGwire KC, Weltz MA, Nouwakpo S, Spaeth K, Founds M, Cadaret E. Mapping erosion risk for saline rangelands of the Mancos Shale using the rangeland hydrology erosion model. *Land Degrad Dev*. 2020;1–13. https://doi.org/10.1002/ldr.3620